PMM/A-231

COMISION NACIONAL DE ENERGIA ATOMICA
DEPENDIENTE DE LA PRESIDENCIA DE LA NACION

PROGRAMA MULTINACIONAL DE METALURGIA
(Programa Regional de Desarrollo Científico y Tecnológico-OEA)

A METHODOLOGY FOR THE PREDICTION OF SUSCEPTIBILITY OF STRESS CORROSION CRACKING

José R. Galvele

III Seminario Latinoamericano en el Nivel de Postdoctorado
Tema: Corrosión

Buenos Aires - Argentina
1977

PMM/A-231

COMISION NACIONAL DE ENERGIA ATOMICA
DEPENDIENTE DE LA PRESIDENCIA DE LA NACION

PROGRAMA MULTINACIONAL DE METALURGIA
(Programa Regional de Desarrollo Científico y Tecnológico-OEA)

A METHODOLOGY FOR THE PREDICTION OF SUSCEPTIBILITY OF STRESS CORROSION CRACKING

José R. Galvele

III Seminario Latinoamericano en el Nivel de Postdoctorado
Tema: Corrosión

Buenos Aires - Argentina
1977

INTRODUCTION

The aim of the present work is to develop a technique to evaluate such parameters as crack propagation rate and crack sharpness through short term experiments. Such a technique would be a useful tool to predict dangerous potentials, alloy structures, heat treatments and/or water composition ranges which might be found in industrial equipment. On the other hand, these short term experiments would make it possible to evaluate the significance of such changes in the working system as the use of inhibitors, contamination by leaking condensers, change in alloy specifications, etc.

The proposed technique is limited to slip dissolution stress corrosion cracking processes. It will not predict such processes as hydrogen embrittlement or liquid metal embrittlement.

So far the technique has been successfully applied to mild steel in nitrate solutions, mild steel in sodium hydroxide solutions, stainless steel in HCl solutions, stainless steel in H_2SO_4 solutions and stainless steel in H_2SO_4 + NaCl solutions. There is also strong evidence that it works for stainless steel in NaOH solutions and for Incolloy 800 in NaOH solutions. From what is known at present about stress corrosion cracking, it should work in most of the stress corrosion cracking cases found in water cooled reactors.

SLIP DISSOLUTION MODEL FOR S.C.C. OF LOW STRENGTH ALLOYS

As it was recently reviewed by Staehle (1), film rupture, as a result of slip process, is the essential condition for stress corrosion cracking initiation, Figure 1. After the film is broken, and the bare metal

is exposed to the solution, subsequent processes are defined by the environmental conditions. Under certain conditions the bare metal repassivates, and the metal retains its corrosion resistance. On the other hand, other circumstances, defined by the electrode potential or by the electrolyte composition, could lead to localized corrosion on the slip steps. A process like that shown in Figure 2 starts, and will eventually lead to the formation of a stress corrosion crack.

As it is an electrochemical process, the depth of attack in Figure 2 can be evaluated from the current density of the straining metal. This will give the rate of crack propagation through the following equation:

$$V = \frac{j \cdot M}{F \cdot z \cdot d} \qquad (I)$$

where V is the crack penetration rate, in cm/s; j is the current density on the slip step, in A/cm^2; M is the atomic weight of the dissolving metal; z is the valence; and d is the density, in g/cm^3. The aim of the present technique is to evaluate j.

When the crack propagation rate, V, can be directly measured, equation (I) will give the current density necessary for the crack to propagate by electrochemical dissolution.

Studies on the pitting of metals showed that localized corrosion on a metal could proceed at rather high current densities. For aluminum, for example, Kaesche (2) reported current densities of 0.3 to 1.1 A/cm^2. For stainless steel Sato et al (3) found limiting current densities of 8 A/cm^2. For iron Vetter and Strehblow (4) reported current densities of 0.9 to 2.0 A/cm^2.

And for small pits in nickel Vetter (5) reported current densities as high as 50 to 70 A/cm^2. This is a matter that requires further study, but the maximum current densities at the bottom of the cracks can be assumed to be somewhat between 1 A/cm^2 and 70 A/cm^2.

Figures 3 and 4 show the effect of stress intensity on the stress corrosion cracking propagation rates (6,7). Figure 3 shows results for high strength aluminum alloys in liquid mercury and in KI solutions. On the right side of the figure the current densities required for the cracks to propagate by electrochemical dissolution are shown. From the very high propagation rates found in liquid mercury electrochemical processes are ruled out. This is not the case for SCC in KI solutions, where the crack propagation rate is in the range of values expected for an electrochemical process.

Figure 4 shows crack propagation rates for various metals. As it is observed, an electrochemical process could account for most of the measured crack propagation rates. Crack propagation rates for Al-Mg-Zn alloys and for Ti alloys are at the top limit of what should be expected for a purely electrochemical process, and the propagation mechanism for those alloys is still a matter of discussion.

CRACK PROPAGATION RATE

The use of continuously straining metal for the study of SCC was introduced by Hoar and West (8) in 1958. These authors found (9) strong depolarization when straining stainless steel in $MgCl_2$ solutions. Hoar and Scully (10) reported current increases when straining stainless steel in $MgCl_2$ at constant potential. Scully and Hoar (11) found a qualitative correlation

between the current increase of the straining metal and its susceptibility to SCC. Whenever a metal was susceptible to SCC high current increases were observed upon straining. On the other hand, metals not susceptible to SCC would not show such current increases.

Hoar and Galvele (12) made a quantitative correlation between current increase and crack propagation rate for mild steel in nitrate solutions. Figure 5 shows the current increase measured during straining mild steel in a $Ca(NO_3)_2$ solution at constant potential. The same results are replotted in Figure 6 as a function of total strain. The current increase was indenpendent of the strain rate, but depended on the total strain. This showed that for the strain rates used by Hoar and Galvele no repassivation of the bare metal took place before the wire was broken. Figure 6 can be used to evaluate the current density on the bare metal and, by means of Equation (I), the crack propagation rate. The bare metal surface is calculated with an equation derived by Bubar and Vermilyea (13):

$$\% \text{ Bare surface} = 100 \left[1 - \left(\frac{\lambda_o}{\lambda} \right)^{1/2} \right] \qquad \text{(II)}$$

where λ_o is the initial specimen length, and λ is the length at any time. The authors derived this equation on the assumptions that the volumes of both the metal and the film were constant, that the film cracked at $\lambda = \lambda_o$, and that the film remained in contact with the metal while the diameter was reduced due to elongation. The authors pointed out that this last assumption required some deformation of the film.

Equation (II) was derived in the following way:

$$\% \text{ Bare Surface} = \% \Delta S = \frac{S - S_o}{S} \times 100 \qquad \text{(III)}$$

The initial surface is given by:

$$S_o = \pi \cdot r_o \cdot \lambda_o$$

and the surface at any time is:

$$S = \pi \cdot r \cdot \lambda$$

The initial volume of the metal is:

$$V_o = \pi \cdot r_o^2 \cdot \lambda_o$$

and since the metal volume is constant:

$$\pi \cdot r_o^2 \cdot \lambda_o = \pi \cdot r^2 \cdot \lambda$$

reordering:

$$\frac{r_o^2}{r^2} = \frac{\lambda}{\lambda_o}$$

and replacing in (III), equation (II) is obtained.

If the elongation is given by:

$$\Delta \lambda_\% = \frac{\lambda - \lambda_o}{\lambda} \times 100$$

the % elongation can be compared with the % bare metal. A good approximation of the value of % bare metal is given by:

$$\% \text{ Bare metal} \approx 1/2 \% \text{ elongation} \qquad \text{(IV)}$$

This approximation is valid for elongations up to 30%, with an error of less than 10% in the calculated bare surface.

In Figure 6 the total current density for 10% elongation is 0.1 A/cm^2. From Equation (IV) the bare metal is 5% of the total surface. The current density on the filmed metal is very small, and can be ignored. So the current density on the bare metal is 2.0 A/cm^2.

From straining mild steel in $Ca(NO_3)_2$ solution, at strain rates of the order of 100 %/min, Hoar and Galvele calculated the current density on the bare metal (Table I, column I). At this high strain rates no cracks were visible at the end of the experiments. At 8%/min, on the other hand, intergranular cracks were observed at the end of the experiments. From the depth of the cracks, and the exposure time, the crack propagation rate was calculated (Table I, column II). A very good correlation between the propagation rates calculated from the straining experiments and the crack propagation rates evaluated from metallographic observations was found.

The work with mild steel in nitrate solutions not only showed that the crack propagation rates could be predicted, but also provided a way for predicting stress corrosion cracking susceptibility under new experimental conditions. Previous publications on the subject indicated that stress corrosion cracking in nitrate solutions was inhibited by NaOH. It was a generally accepted fact that no SCC could occur in alkaline nitrate solutions. Nevertheless the straining experiments showed that even at high pH values SCC was possible. At the corrosion potential, -0.22 V(nhe), no

SCC was detected in 4 M $NaNO_3$ at pH 10.3. Nevertheless, if the potential was increased up to -0.14 V(nhe), severe SCC was predicted and actually found.

The same technique was used by Hoar and Jones (14) for the study of SCC of mild steel in boiling 10 N NaOH solutions. These authors measured the current density of the bare metal using strain rates higher than 100 %/min, and compared the results with metallographic measurements of cracks found at 1.5 %/min, Table II. Very good correlation was found between both values.

In the papers by Hoar and Galvele, and by Hoar and Jones, the initial current density was very small compared with the current density during straining. So the initial current density was ignored in the calculation of the current density on the bare metal. But this is not always the case, as determined by Galvele et al (15) when studying stainless steel in HCl solutions, Figure 7. AISI 304 stainless steel is susceptible to SCC in HCl solutions near the corrosion potential. The straining experiments proved that an initial cathodic current on the static metal could lead to an anodic current on the straining metal. In such a case the current density on the bare metal was calculated in the following way:

At -0.160 V the stationary current density for AISI 304 stainless steel in 1N HCl solution was -1.5×10^{-5} A/cm^2 (cathodic). After 30% elongation the current density was 1.7×10^{-5} A/cm^2 (anodic). If the change in current density is attributed to the reaction taking place on the bare surface (ca. 15% of the total area) then we have:

$$(i_s \times A_s) + (i_b \times A_b) = i_y$$

i_s being the current density on the static metal; A_s the fraction of area

covered by a film; i_b the current density on the bare metal; A_b the fraction of area of bare metal; and i_y the current density on the straining metal. For the above mentioned example we have:

$$\left[\left(-1.5 \times 10^{-5}\right) \times 0.85\right] + \left(i_b \times 0.15\right) = 1.7 \times 10^{-5}$$

and:

$$i_b = 2.0 \times 10^{-4} \text{ A/cm}^2.$$

Figures 8 and 9 show the current densities at different potentials for the stationary metal and for the bare metal.

Very good correlation was found between the crack propagation rates calculated after straining the metal for about 10 seconds, and those measured on U-bend specimens exposed for several weeks at constant potential.

CRACK SHARPNESS RATIO

Hoar and Jones (14) found that the crack propagation rate was not sufficient in itself to define a system from the SCC point of view. Mild steel shows SCC in 10N NaOH between -0.85 and -0.55 V(she). At higher potentials no SCC is observed. Nevertheless, Hoar and Jones found high bare metal current densities at potentials over -0.4 V. Figure 10 shows the current density at fracture, which is proportional to the current density on the bare metal. In the same figure the current density on the static metal is shown. It was found that in the range of maximum SCC susceptibility the current density on the static metal is very low. Under such conditions, while the straining metal at the bottom of the crack dissolves rapidly, the rest of the metal, including the static sides of the crack, will dissolve very slowly. In

this way sharp stress corrosion cracks will be obtained. If the potential is increased the crack propagation rate decreases, and then starts to increase again. Nevertheless, the current density on the static metal also starts to increase. This leads to a generalized dissolution, and no sharp cracks will be formed. In a qualitative way, Hoar and Jones defined the regions of SCC susceptibility using the ratio of currents, as shown in Figure 11. SCC only occurs where a high current ratio is found.

Similar observations were made by Galvele et al (15) for AISI 304 in HCl solutions. These authors found that a quantitative correlation could be made if instead of using the current density at fracture, the net anodic current density on the bare metal was used. In this way Galvele et al developed a SCC diagram where the penetration rate and the current ratio were shown as a function of potential, Figure 12. From Figure 12 Galvele el at could predict the crack morphology and the crack penetration rate for AISI 304 in 1N HCl solution. These predictions were confirmed with U-bend specimens (Figures 13 and 14) and were in good concordance with the SCC ranges reported by Bianchi et al (16).

The use of these diagrams was extended by Maier and Galvele (17) to the study of SCC of AISI 304 in H_2SO_4 solutions and in H_2SO_4 + NaCl solutions. Figures 15, 16 and 17 show the SCC diagrams for AISI 304 in 5N H_2SO_4; in 1N H_2SO_4 + 0.1N NaCl; and in 5N H_2SO_4 + 0.5N NaCl solutions. The triangles indicate the penetration rates metallographically measured from long exposure specimens. As it is observed, good correlation was found between the short term straining experiments and the long exposure experiments. No SCC has been reported so far for AISI 304 in 5N H_2SO_4 solutions. In agreement with this, Figure 15 shows that the penetration rate will be high, but that the

crack sharpness ratio will be very small. Then between 0 and -0.10 V generalized corrosion should be expected for AISI 304 in this solution. S.E.M. shows that (Figure 18) trenches are initiated, but the corrosion rate on the static metal is so important that no fissures could be formed. Maier and Galvele found that for crack sharpness ratios lower than 5 no cracks are detected in any of the so far studied systems.

In 1N H_2SO_4 + 0.1N NaCl solution, at potentials below -0.050V, cracks should appear, since the current ratio becomes higher than 5, Figure 16. In this solution the crack propagation rate will not be very much affected by the potential, and will be, on the whole, slower than that found in a 1N HCl solution.

Staehle (18) reported that, from the SCC point of view, the 5N H_2SO_4 + 0.5N NaCl solution is far more aggressive than the 1N H_2SO_4 + 0.1N NaCl solution. This is also found by comparing Figures 16 and 17. While the current ratio is similar in both solutions, the propagation rate is far more rapid in the second solution than in the 1N H_2SO_4 + 0.1N NaCl solution. From Figures 15 and 17 it was concluded that adding 0.5 N NaCl to the 5N H_2SO_4 solution SCC of AISI 304 should appear, a prediction confirmed by S.E.M., Figure 18 and 19.

Preliminary experiments by Maier and Galvele show that at the pitting potential of a metal, a diagram like that in Figure 20 should be found when no SCC occurs, and diagrams like in Figure 21, when there is SCC susceptibility.

REPASSIVATION RATE

As pointed out by Smith and Staehle (19) one important parameter in the slip dissolution SCC process is the repassivation rate of the bare metal on the slip steps, Figure 1. If the bare metal repassivates very easily, the oxide film is reformed on the slip steps, and no noticeable corrosion takes place. On the other hand, if repassivation is slow, localized corrosion begins on the slip steps, eventually leading to SCC. Figure 5 shows an example of a slow repassivation process. From Figure 6 it is concluded that under a strain rate of 31 %/min, repassivation of the slip steps, for mild steel in 4N $Ca(NO_3)_2$ solution, takes more than 20 seconds to occur. Before repassivation starts, the current increases linearly with the total strain, as shown in Figure 6. As soon as repassivation starts the current density reaches a saturation point, Figure 22. This current was called "average saturation current" (a.s.c.), and was studied by Murata and Staehle (20). The a.s.c. is function of the strain rate. The higher the strain rate, the higher tha a.s.c.

One example of fast repassivation rate is found with aluminum in NaCl solutions below the pitting potential (21). Figure 23 shows that a potential independent a.s.c. is obtained. This current is shown in Figure 24 for different strain rates. Below the pitting potential (E_p) no corrosion is detected on the strained metal. Figure 25 shows that the a.s.c. is a linear function of the strain rate. It follows the empirical relation:

$$i = (1 \times 10^{-6}) + (2.11 \times 10^{-5} \times \dot{\epsilon}) \qquad (V)$$

where i is the current density in A/cm^2, and $\dot{\epsilon}$ is the strain rate in min^{-1}.

To define the SCC susceptibility of a system it is necessary to have a value for critical repassivation rate. So far there has been no evaluation of the repassivation rate below which SCC occurs, and over which the metal is immune to SCC.

In the measurements by Hoar et al (12,14) and by Galvele et al (15,16) the idea of a critical repassivation rate is implicit in the choice of the range of strain rates. Hoar and Galvele (12) found that no repassivation was taking place when straining mild steel in nitrate solutions at strain rates from 8 %/min to 307 %/min. Hoar and Jones (14), on the other hand, found that for mild steel in NaOH solutions the repassivation rate became important below 100 %/min. They concluded that the repassivation rate for that solution was higher than that for the nitrate solutions. One would be tempted to suggest that higher strain rates should be used so as to include systems of higher repassivation rates. Nevertheless a very high strain rate would lead to erroneous propagation rates. Staehle and Turtler (22) used strain rates of 750 %/sec in their experiments. According to equation (V), this strain rate would give a current density on the bare metal of 9.5×10^{-3} A/cm^2 for aluminum. This current density is equivalent to a crack propagation rate of 3.28×10^{-7} cm/s, and would give propagation rates similar to those found for SCC of mild steel in NaOH solutions, Nevertheless, no such SCC has been found for pure aluminum in NaCl solutions.

From the measurements by Galvele et al for stainless steel in acid chloride solutions, it comes out that strain rates of 40 %/min are adequate for that system. In principle it can be concluded that a strain rate somewhere between 40 %/min and 200 %/min would be adequate for the present technique. Nevertheless it would be necessary to find a mechanistic explanation

to supoort this election. Theoretically the strain rate used would be that shown by the metal at the bottom of the crack. This value will change with the stress intensity, and an evaluation of the most common strain rates should be necessary.

Following this same line of thought, we can compare the influence of stress intensity on SCC velocity, Figure 26, with the influence of strain rate on the current density. Assuming that similar processes take place in the SCC of aluminum and of mild steel, we could conclude that while the rate-determining process in Region I is the strain rate at the bottom of the crack, the rate-determining process in Region II is the metal dissolution rate.

SCC OF AISI 304 IN NaOH SOLUTIONS

Subrahmanayam and Staehle (23) studied the SCC morphology in AISI 304 exposed to boiling 60% NaOH solution, Figure 28. These authors found that the morphology of the cracks was strongly dependent on the electrode potential. The same was observed with the failure time. The authors also found that the failure time was related to the maximum recorded current densities, Figure 29. No information is available to evaluate the crack propagation rates or the currend density ratios. Current-time curves for this system show an initial increase in the current density, followed by a slow decrease. The initial increase could be the result of undermining the air-formed oxide film by the NaOH solution. In this way, the maximum current density could be taken as a rough evaluation of the bare metal current density. As shown in Figure 29, the higher the bare metal current density, the shorter the failure time. If the current ratio is calculated, it changes with the potential, and

different morphologies should be expected at different potentials. It can be concluded that the technique described in the present paper should be applicable to the evaluation of SCC susceptibility of AISI 304 in NaOH solutions.

In a similar way it seems that it is applicable to AISI 410, AISI 430, Incoloy alloy 800, Inconel alloy 600, 618C, and 619C in 70% boiling NaOH solutions (24).

FUTURE WORK

A major effort should be done to define the following parameters:

1.-STRAIN RATE. Define the most convenient strain rate for SCC tests. Apparently the most suitable value would be somewhere between 40 %/min and 200 %/min.

2.-MINIMUM CRACK PROPAGATION RATE. It is necessary to know the minimum crack propagation rate below which SCC becomes irrelevant. According to Speidel (6) a practical limit would be around 10^{-9} or 10^{-10} m/s. This would require current densities of the order of 10^{-3} or 10^{-4} A/cm^2 on the bare metal.

3.-CRACK SHARPNESS RATIO. It is necessary to evaluate the minimum crack sharpness ratio below which no stress corrosion cracks are formed. In preliminary experiments (17), $i_b/i_s = 5$ was found as the minimum ratio for SCC susceptibility.

REFERENCES

1.-R.W.Staehle. INTERNATIONAL CONFERENCE ON STRESS CORROSION CRACKING AND HYDROGEN EMBRITTLEMENT OF IRON BASE ALLOYS. Firminy, France 1973.

2.-H.Kaesche. Z. physik. Chem. N.F., 34, 87 (1962).

3.-N.Sato, T.Nakagawa, K.Kudo and M.Sakashita. Trans. Japan Inst. Metals, 13, 103 (1972).

4.-K.J.Vetter and H.H.Strehblow, Ber. Bunsenges. physik. Chem. 74, 1024 (1970).

5.-K.J.Vetter, private communication.

6.-M.O.Speidel. THE THEORY OF STRESS CORROSION CRACKING IN ALLOYS (Ed.J.C. Scully),NATO, 1971, p.289.

7.-D.A.Vermilyea. Id. Reference (1).

8.-T.P.Hoar and J.M.West. Nature, 181, 835 (1958).

9.-T.P.Hoar and J.M.West. Proc. Roy.Soc. A 268, 304 (1962).

10.-T.P.Hoar and J.C.Scully. J.Electrochem.Soc. 111, 348 (1964).

11.-J.C.Scully and T.P.Hoar. 2nd. International Congress on Metallic Corrosion, NACE, Houston, 1966, p.184.

12.-T.P.Hoar and J.R.Galvele. Corrosion Sci. 10, 211 (1970).

13.-S.F.Bubar and D.A.Vermilyea. J.Electrochem.Soc. 113, 892 (1966).

14.-T.P.Hoar and R.W.Jones. Corrosion Sci. 13, 725 (1973).

15.-J.R.Galvele, S.R.de Wexler and I.Gardiazabal. Corrosion 31, 352 (1975).

16.-C.Bianchi, F.Mazza and S.Torchio. Corrosion Sci. 13, 165 (1973).

17.-I.Maier and J.R.Galvele. JAPAN-USA SEMINAR ON PASSIVITY AND ITS BREAKDOWN ON IRON AND IRON BASE ALLOYS, Honolulu, Hawaii, March 1975.

18.-R.W.Staehle. Private communication.

19.-T.J.Smith and R.W.Staehle. Corrosion 23, 117 (1967).

20.-T.Murata and R.W.Staehle. 5th INTERNATIONAL CONGRESS ON METALLIC CORROSION. Japan. NACE 1974.

21.-S.B.de Wexler and J.R.Galvele. J.Electrochem.Soc. 121, 1271 (1974)

22.-R.W.Staehle and G.Turtler. Grant N° SRG/SCC-003. Final Report, NATO 1975.

23.-D.V.Subrahmanayam and R.W.Staehle. See: R.W.Staehle, Reference (6),p.228; or: A.K.Agrawal and R.W.Staehle. Report N° COO-2018-24, U.S.Atomic Energy Commission, p. 8.

24.-E.L.Liening and R.W.Staehle. See: E.L.Liening, EFFECT OF STRESS, TEMPERATURE, AND POTENTIAL ON CORROSION OF TYPES 410 AND 430 STAINLESS STEELS, INCOLOY ALLOY 800, INCONEL ALLOY 600, 618C AND 619C IN 70% NaOH. Thesis 1974 MS L 719 (O.S.U.).

TABLE I. CURRENT DENSITY AT NEW EXPOSED METAL IN FISSURES IN THE OXIDE FILM PRODUCED BY TRACTION, COMPARED WITH CURRENT DENSITY REQUIRED TO ADVANCE "CRACKS" IN THE METAL AT MICROSCOPICALLY MEASURED RATE

Hoar and Galvele Ref(12)

Solution	Potential [V(nhe)]	Initial pH	I C.D. measured (A/cm²)	Time to fracture (s)	Average depth of "cracks" at fracture (μm)	II C.D. required (A/cm²)
4N $Ca(NO_3)_2$	− 0·10	3·7	2·01	35	25	2·08
4N $NaNO_3$	− 0·14	4·8	1·48	77	32·5	1·21
4N $NaNO_3$	− 0·18	4·8	0·80	84	20	0·69
4N $NaNO_3$	− 0·22	4·8	0·26	93	5	0·16
4N $NaNO_3$ + NaOH	− 0·14	10·3	1·32	76	19	0·73

TABLE II. INFLUENCE OF POTENTIAL ON INCIDENCE AND PENETRATION OF CRACKS IN 0·1%C STEEL IN 10M NaOH. 121°C. STRAIN RATE 1·5%/min

Potential (V(she))	Incidence of attack	Current density over bare surface (mA/cm²)	Penetration Calculated from cd (μm)	Penetration Measured microscopically (μm)
—0·50	Some short, blunt pits; no cracks	—	0	0
—0·55	A few cracks	33	10	17–29
—0·60	A few cracks	77	25	23–29
—0·65	A few cracks	74	25	26–34
—0·70	Many cracks—about ½ of grain boundaries penetrated	89	30	29–37
—0·75	Many cracks over ½ of surface	120	40	29–40
—0·80	Many cracks—almost every grain boundary penetrated	154	50	31–40
—0·825	A few cracks	73	25	7–14
—0·85	A few cracks and pits	110	37	3–9
—0·90	No cracks	—	0	0

Hoar and Jones, Ref (14)

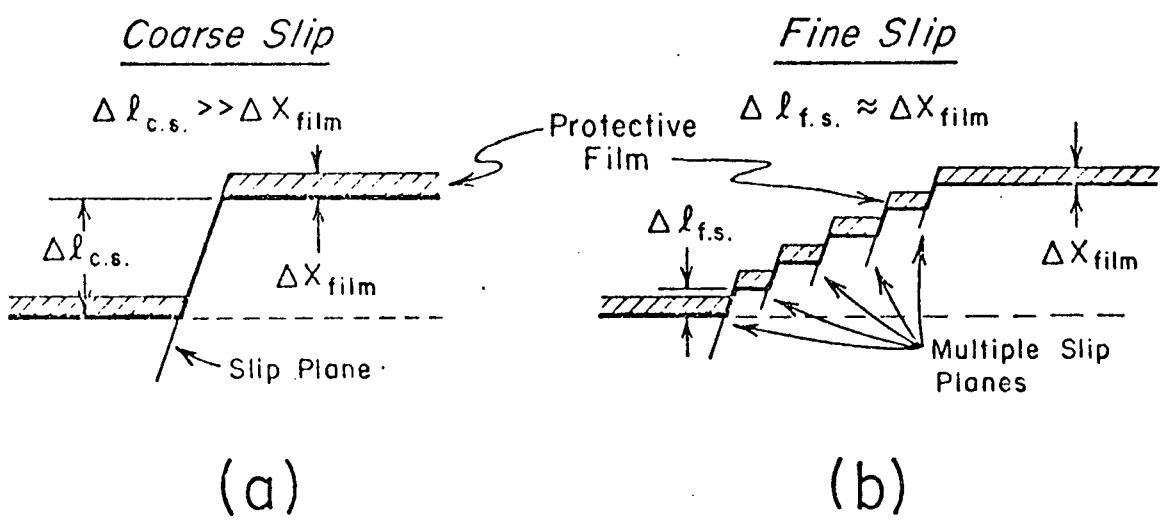

Figure 1. Comparison of slip step heights with thickness of protective films:

(a) Coarse slip, step height >> thickness of film
(b) Fine slip, step height ≈ thickness of film

(R.W.Staehle, ref.(1)).

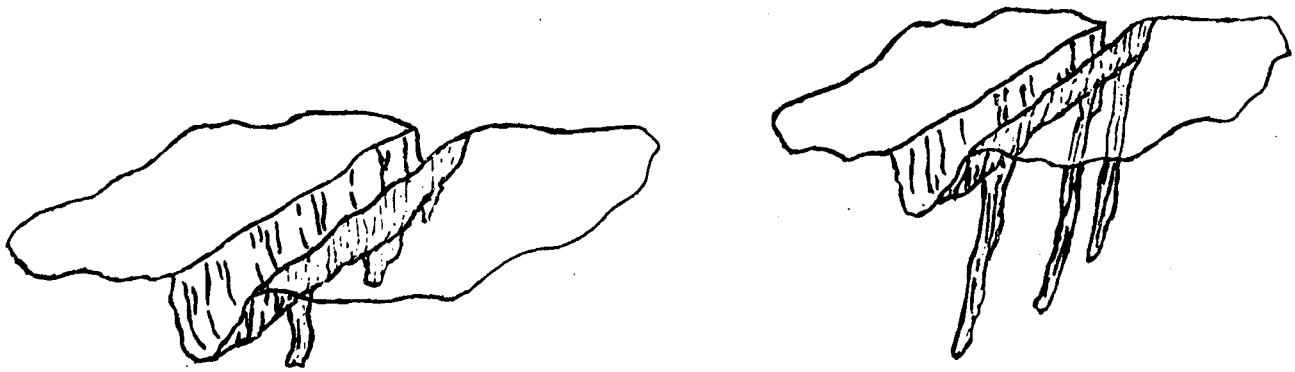

Figure 2. Schematic figure of tunnels extending from dissolution trench. (R.W.Staehle, Ref (1)).

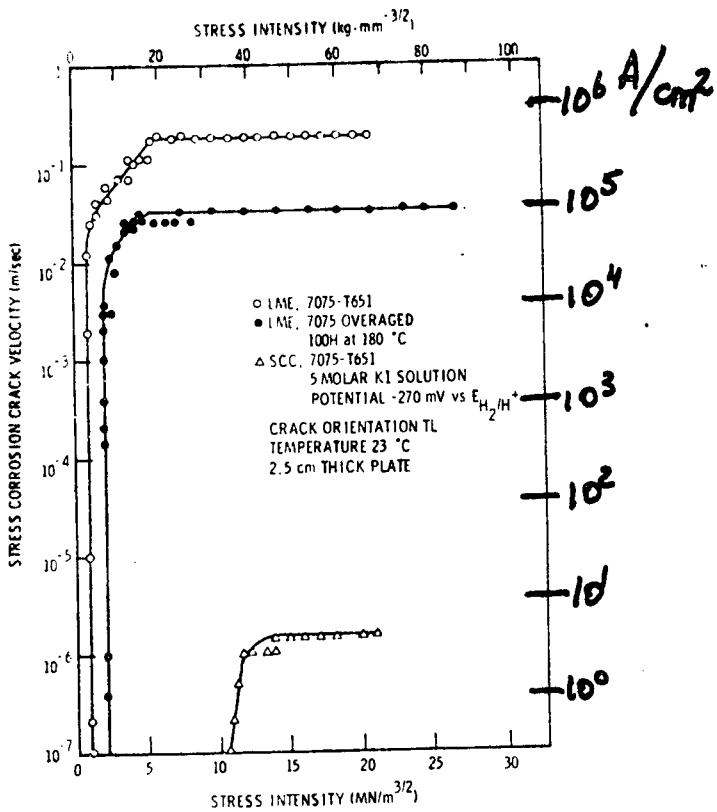

Effect of stress intensity on the velocity of SC cracks filled with liquid mercury and with aqueous iodide solution

FIGURE 3. M.O.Speidel,Ref (6).

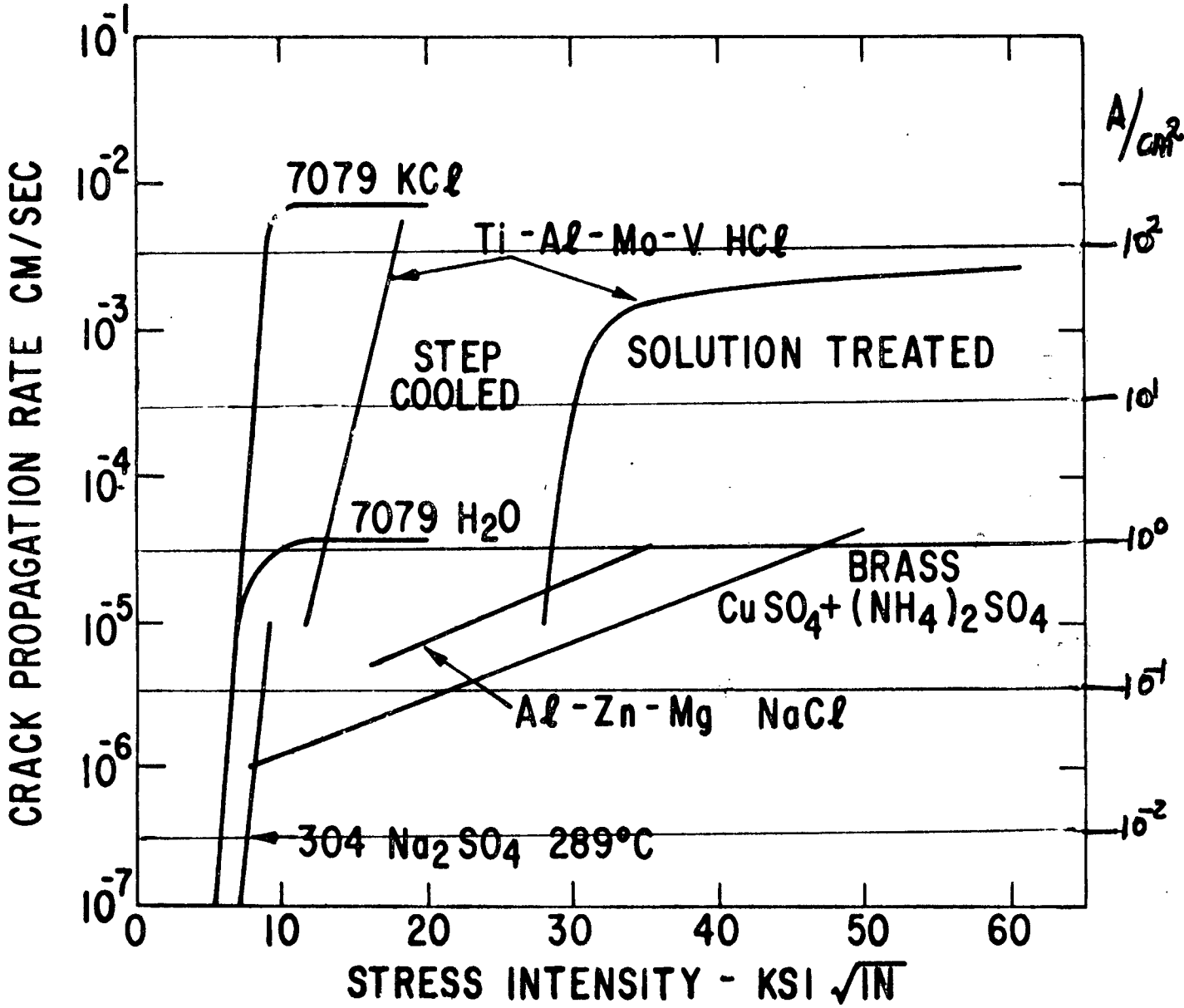

FIGURE 4. Effect of stress intensity on the velocity of stress corrosion cracks in aqueous solutions. D.A.Vermilyea. Ref.(7).

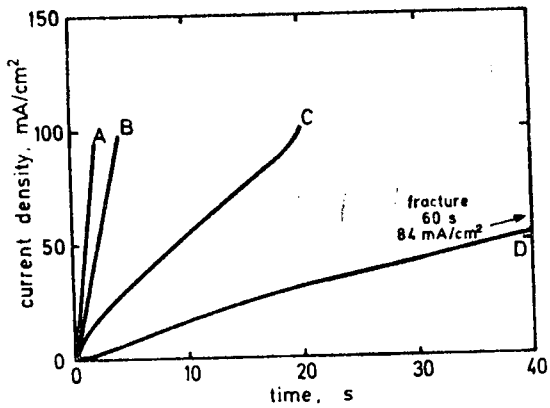

FIG. 5. Potentiostatic current-density/time curves for oxide-covered mild steel yielding at different strain rates in hot calcium nitrate solution.
4N $Ca(NO_3)_2$, pH 3·7 (at 25°C), 102°C, e_H — 0·10V.
Strain rate: A, 307%/min; B, 154%/min; C, 31%/min; D, 8%/min.
Hoar and Galvele, Ref(12).

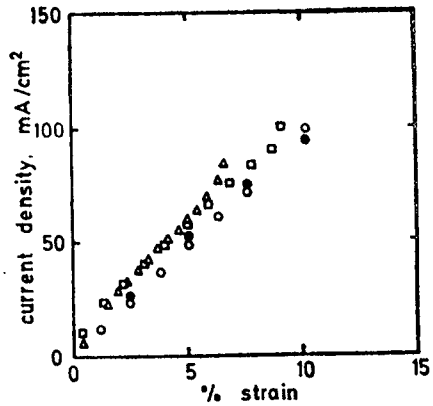

FIG. 6. Variation of current density with % strain (data from Fig. 6.)
4N $Ca(NO_3)_2$, pH 3·7 (at 25°C), 102°C, e_H —0·10V.
Strain rate: ●, 307%/min; ○, 154%/min; □, 31%/min; △, 8%/min.
Hoar and Galvele, Ref.(12).

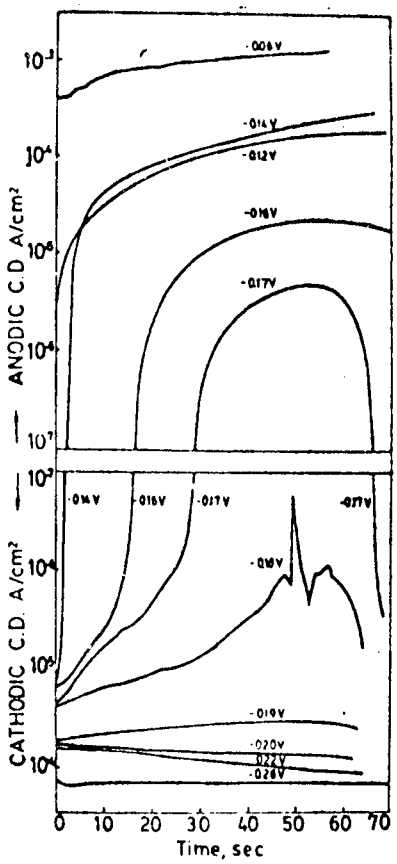

Fig 7: Current-time curves, at constant potential, for straining AISI 304 in deaerated 1M HCl solution at 25°C. Strain rate: 40 %/min. **Galvele et al. Ref.(15)**

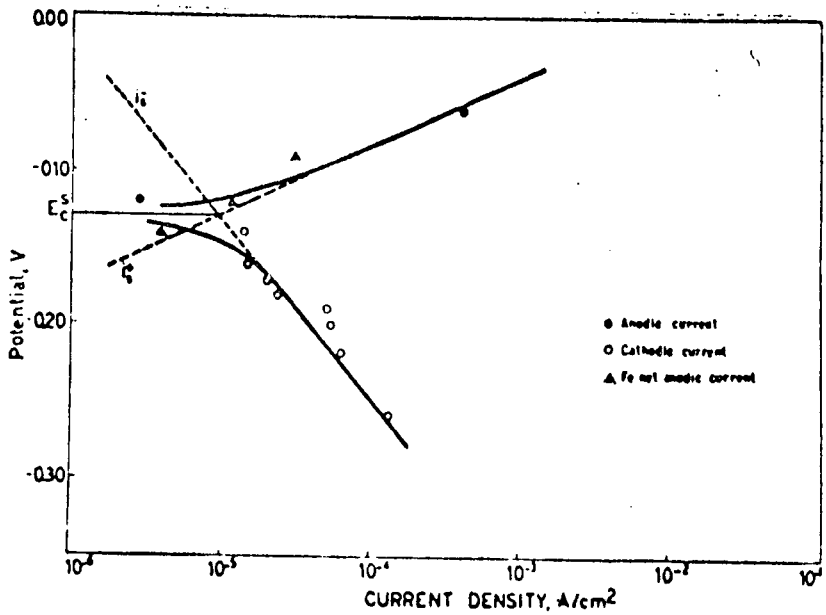

Fig 8: Polarization curve for static AISI 304 in 1M HCl solution at 25°C. i_s^+: Stationary metal net anodic current density. i_s^-: Stationary metal net cathodic current density. E_c^s: Stationary metal corrosion potential. **Galvele et al. Ref.(15).**

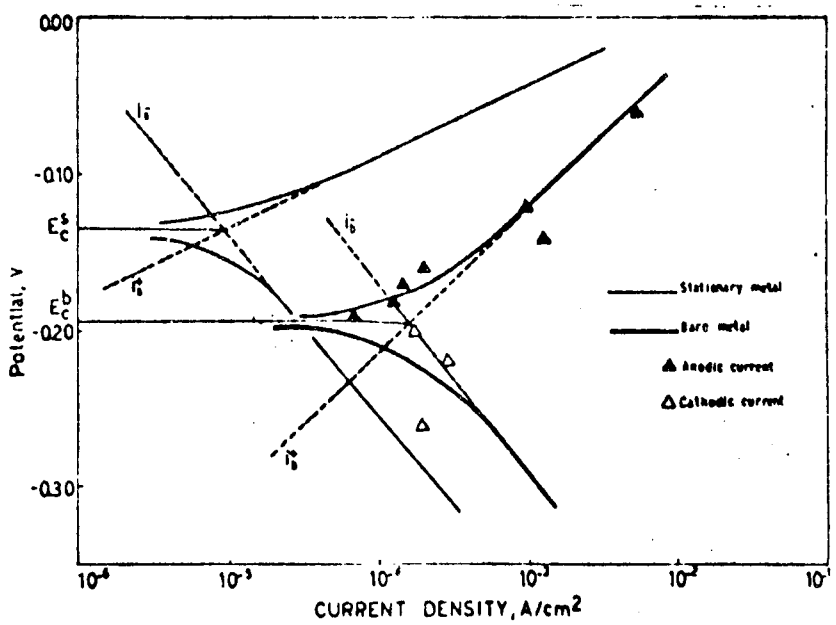

Fig 9: Bare metal calculated polarization curve for straining AISI 304 in deaerated 1M HCl solution at 25°C. i_b^+: Bare metal net anodic current density. i_b^-: Bare metal net cathodic current density. i_s^+: Stationary metal net anodic current density. i_s^-: Stationary metal net cathodic current density. E_c^s: Stationary metal corrosion potential. E_c^b: Bare metal corrosion potential. **Galvele et al. Ref.(15).**

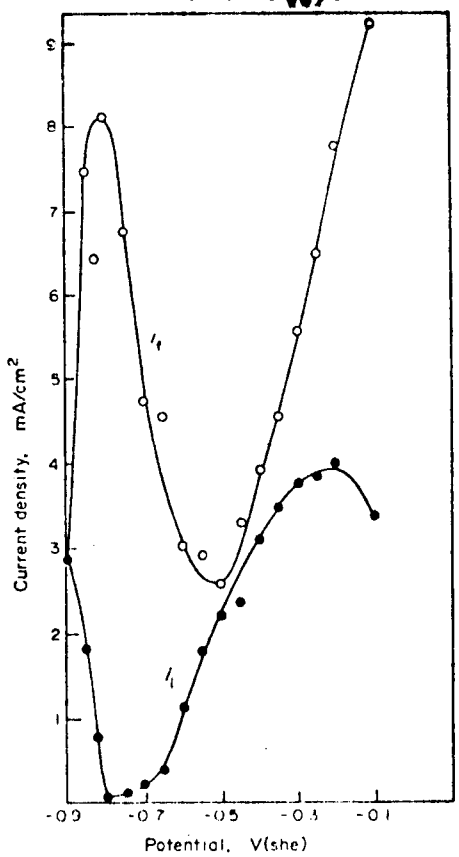

FIG. 10. Influence of potential on cd at fully filmed surface after 40 min polarization i_i, and at fracture of specimen, i_f.
0·1% C steel. 10M NaOH. 121°C. Strain rate 28%/min. **Hoar and Jones, Ref.(14).**
●, c.d. after 40 min polarization, i_i
○, c.d. at fracture, i_f.

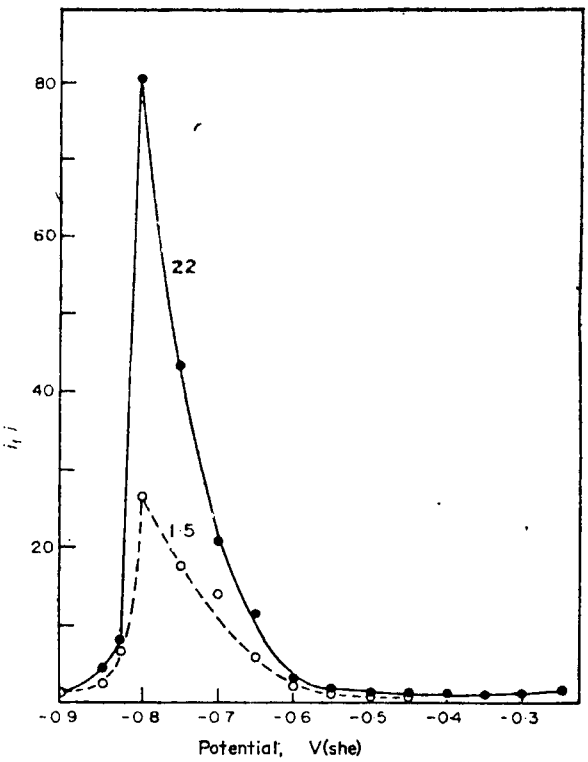

FIG. 11. Variation of ratio i_1/i_1 with potential.
0·1% C steel. 10M NaOH. 121°C.
Hoar and Jones, Ref.(14).

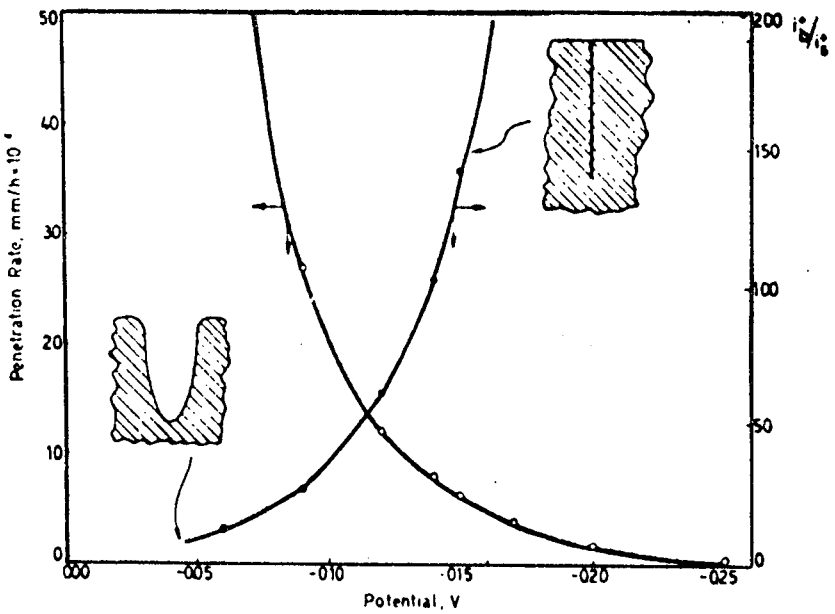

Fig 12 : Calculated crack penetration rate and bare metal to filmed metal current density ratio (i_b^+/i_s^+), as a function of potential for stressed AISI 304 in 1M HCl solution at 25°C. Inscrt: Expected fissure morphology. **Galvele et al. Ref.(15).**

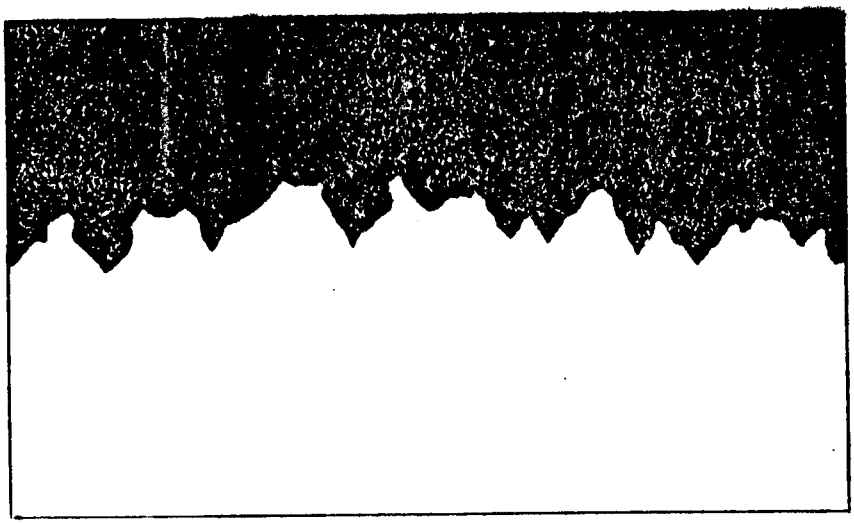

Fig 13 : Uneven general corrosion for stressed AISI 304 in 1M aerated HCl solution at -0.050 V and 25°C, 30 h exposure. Cross-section, 400 X. Galvele et al. Ref.(16). i_b^+/i_s^+ = ca. 10.

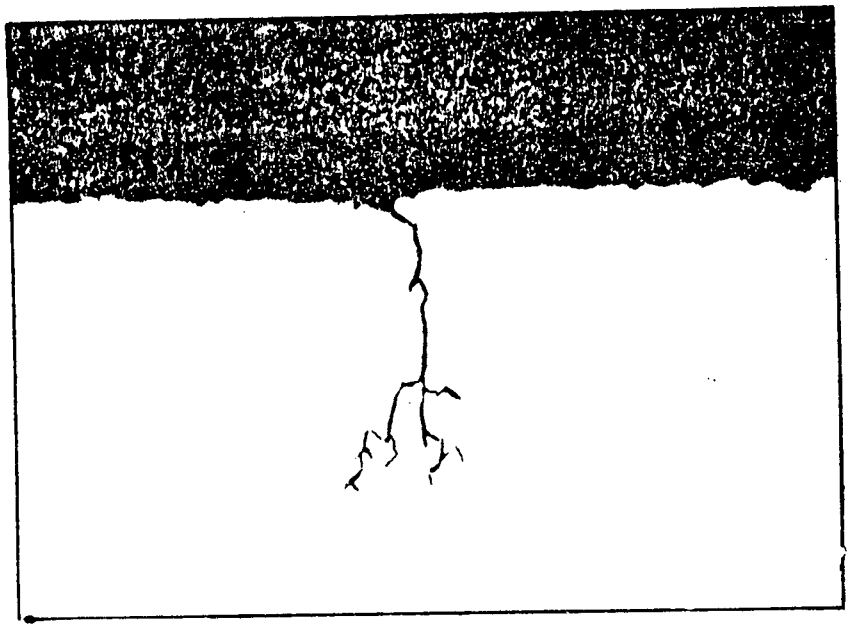

Fig 14 : SCC for AISI 304 stainless steel in 1M solution at -0.150 V and 25°C, 206 h exposure. section, 400 X. Galvele et al.Ref.(15). i_b^+/i_s^+ = ca. 150.

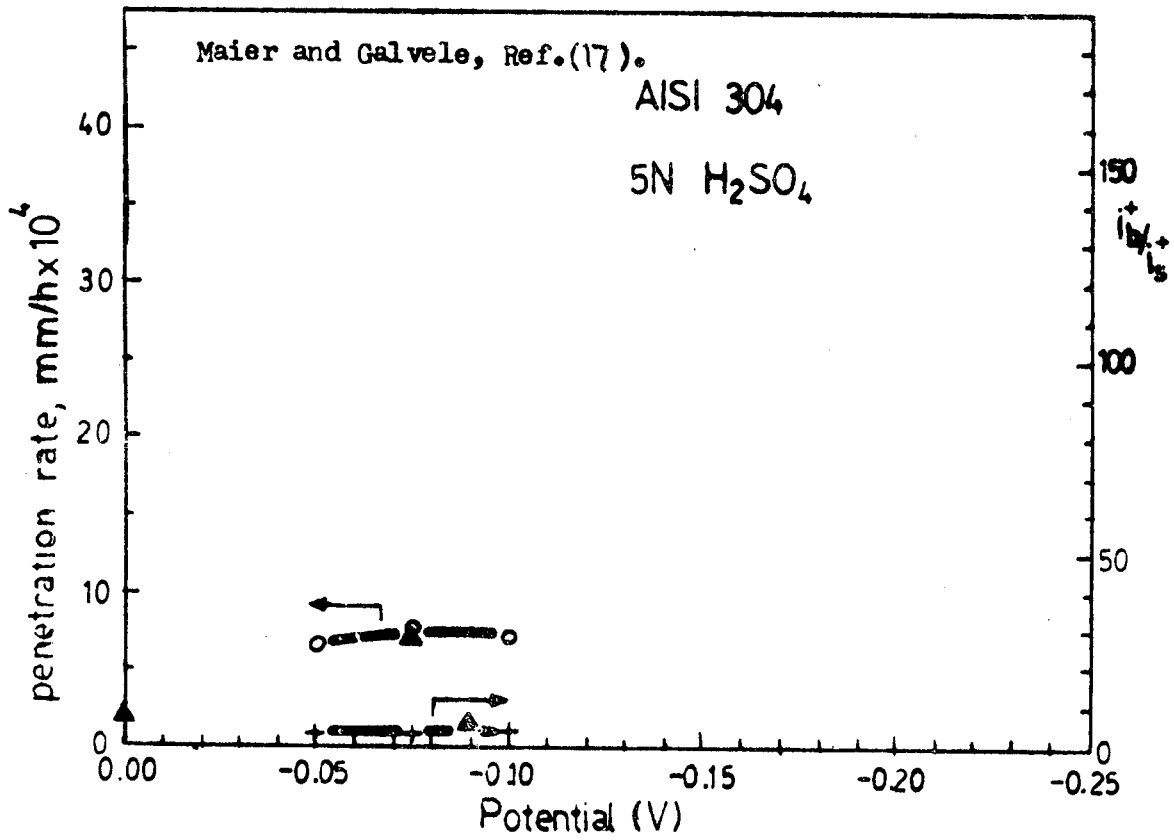

FIGURE 15. Crack penetration rates and bare metal-filmed metal net-anodic-current-density-ratios for AISI 304 austenitic stainless steel 5N H_2SO_4 solution. (▲): Penetration rates measured on U-bent specimens.

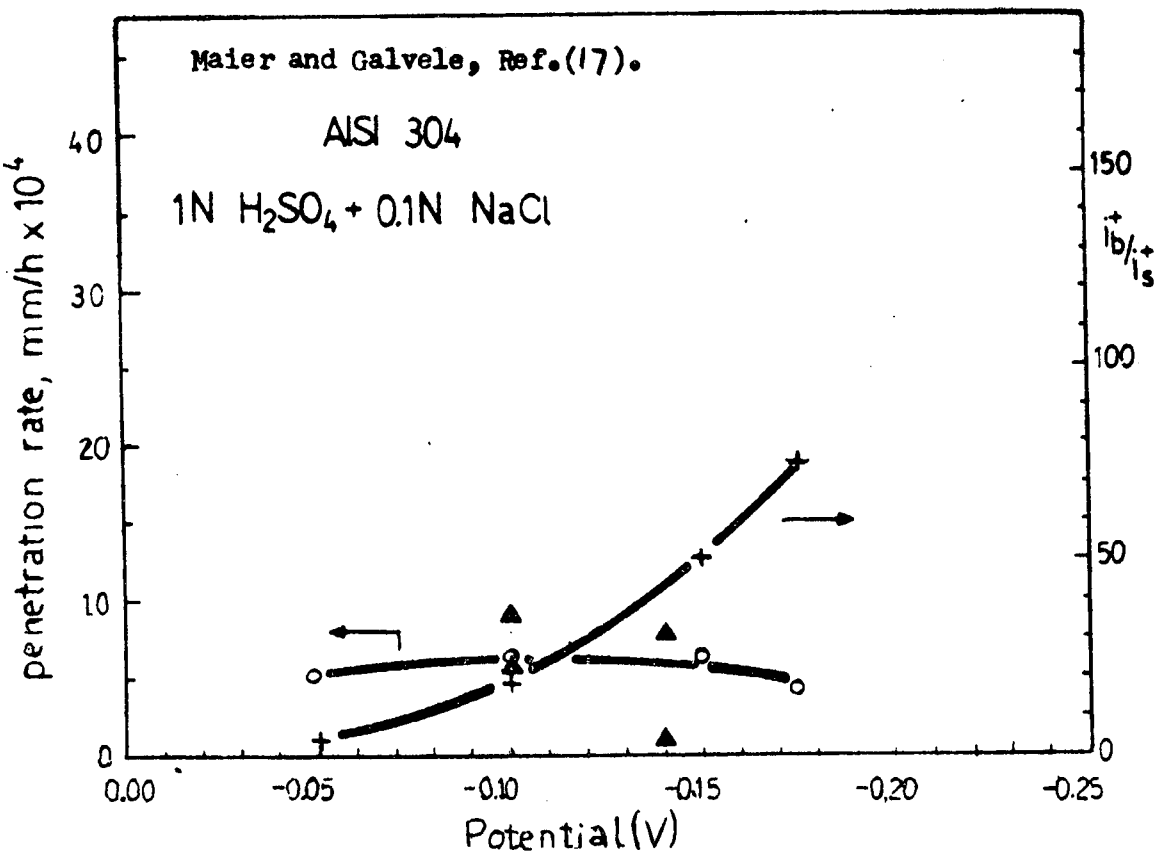

FIGURE 16 Crack penetration rates and bare metal-filmed metal net-anodic-current-density-ratios for AISI 304 austenitic stainless steel in 1N H_2SO_4 + 0.1N NaCl solution. (▲): Penetration rates measured on U-bent specimens.

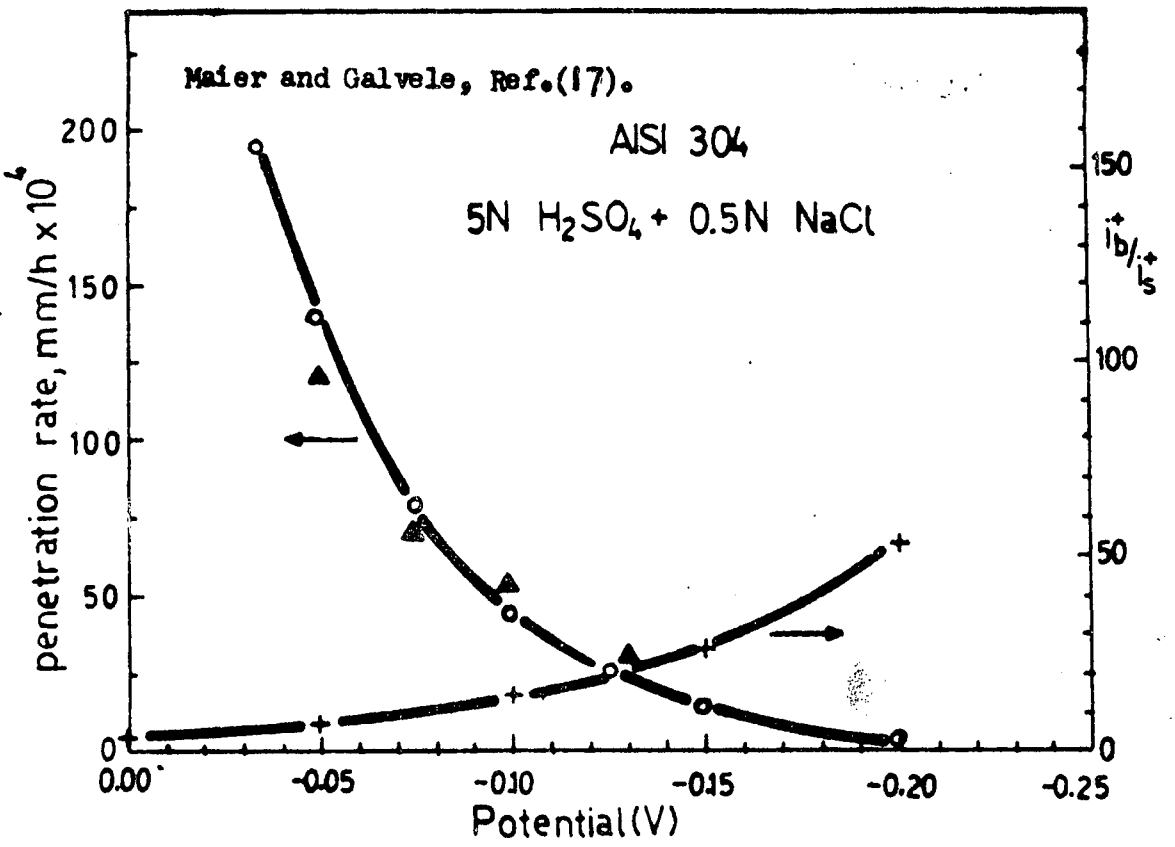

FIGURE 17. Crack penetration rates and bare metal-filmed metal net-anodic-current-density-ratios for AISI 304 austenitic stainless steel in 5N H_2SO_4 + 0.5N NaCl solution. (▲): Penetration rates measured on U-bent specimens.

Maier and Galvele, Ref.(17).

FIGURE 18. Scanning electron micrograph of stressed AISI 304 austenitic stainless steel exposed to 5N H_2SO_4 solution, at a potential of -0.110 V(nhe), during 4 h. U-bent specimen.

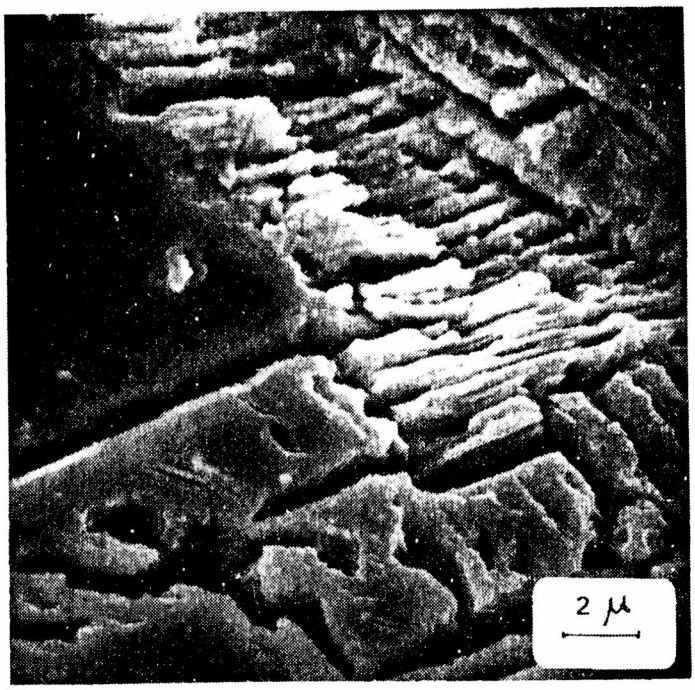

Maier and Galvele, Ref.(17).

FIGURE 19. Scanning electron micrograph of stressed AISI 304 austenitic stainless steel exposed to 5N H_2SO_4 + 0.5N NaCl solution, at a potential of -0.075 V(nhe), during 2 h. U-bent specimen.

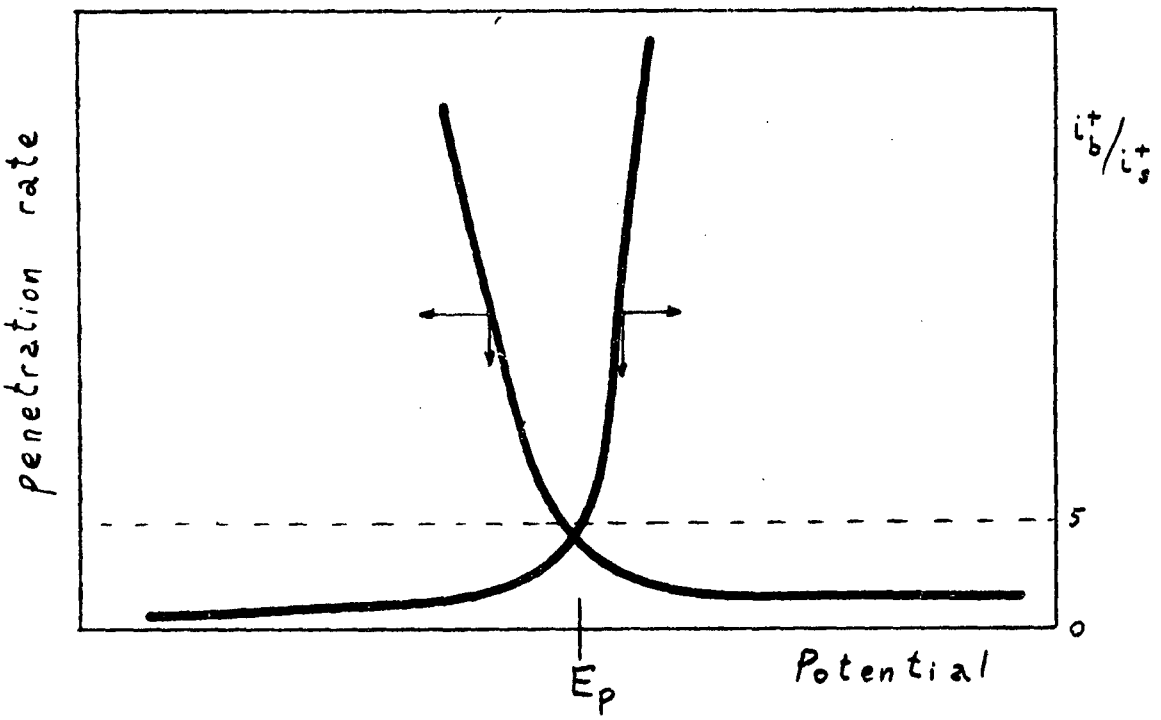

Figure 20. Metal immune to stress corrosion cracking at the pitting potential. (Maier and Galvele).

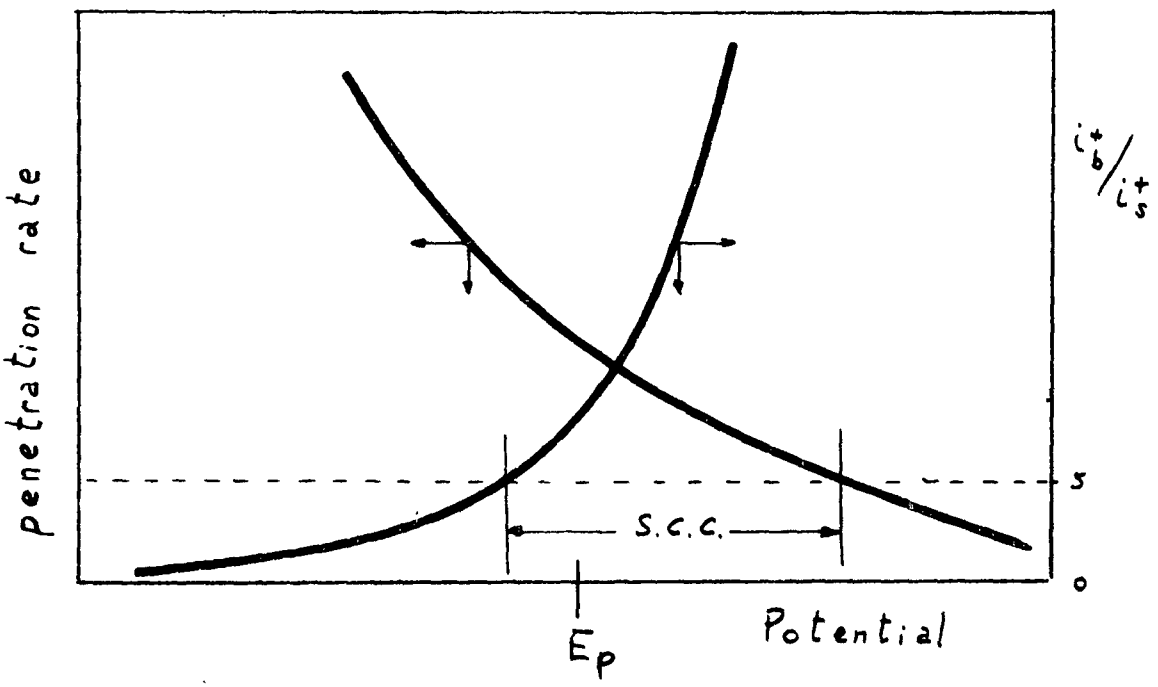

Figure 21. Metal susceptible to stress corrosion cracking at the pitting potential. (Maier and Galvele).

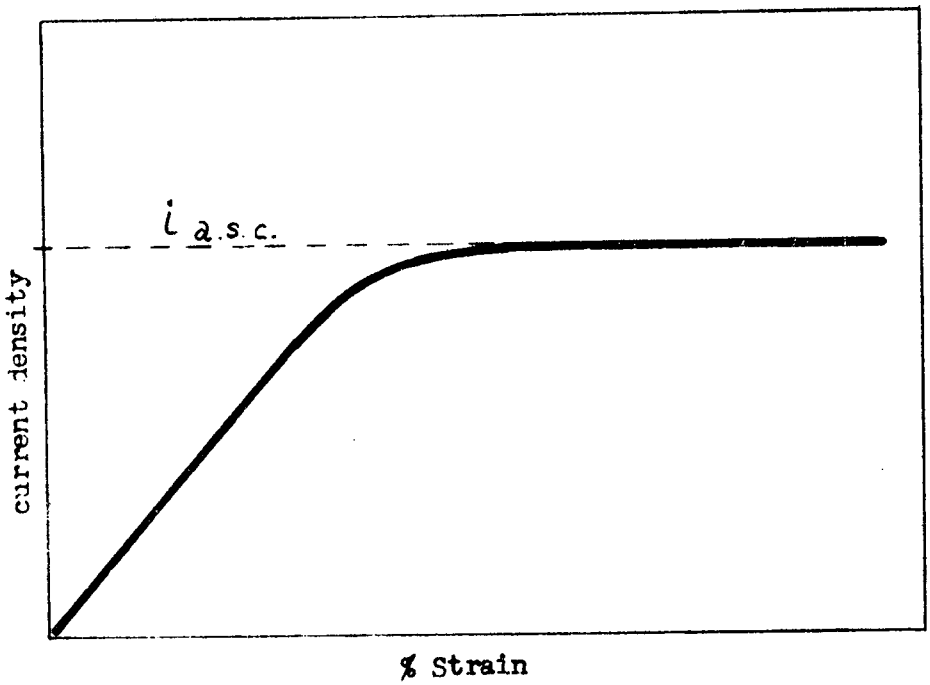

FIGURE 22. Average saturation current due to repassivation of slip steps, for either high repassivation rates or slow strain rates.

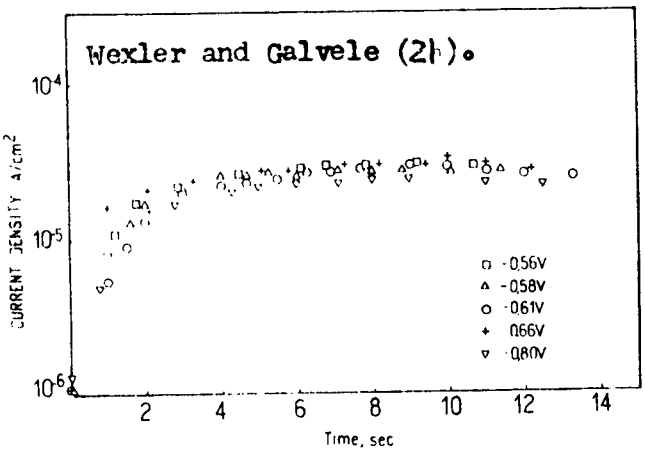

Fig. 23 Potentiostotic current density/time curves at various potentials for aluminum straining at 90%/min in 1M NaCl solution.

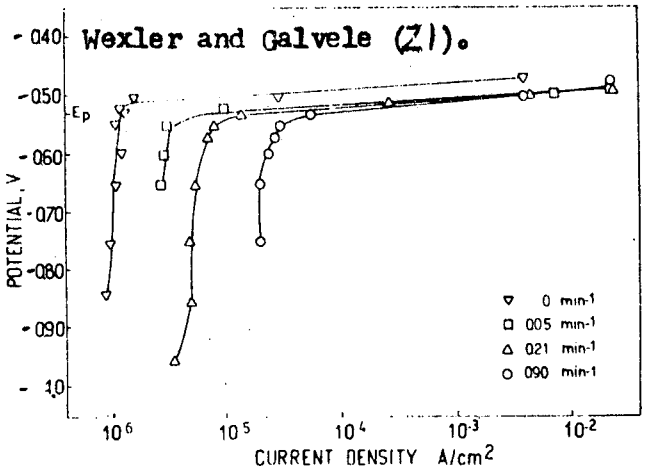

Fig.24 Steady-state current densities for aluminum during straining in 1M NaCl solution at different patentials and at different strain rates.

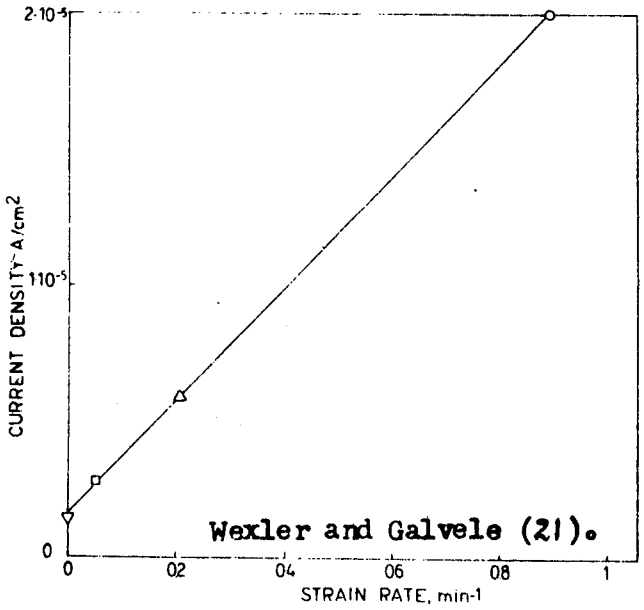

Fig.25 Relation between steady-state current density and strain rate for aluminum straining in 1M NaCl solution.

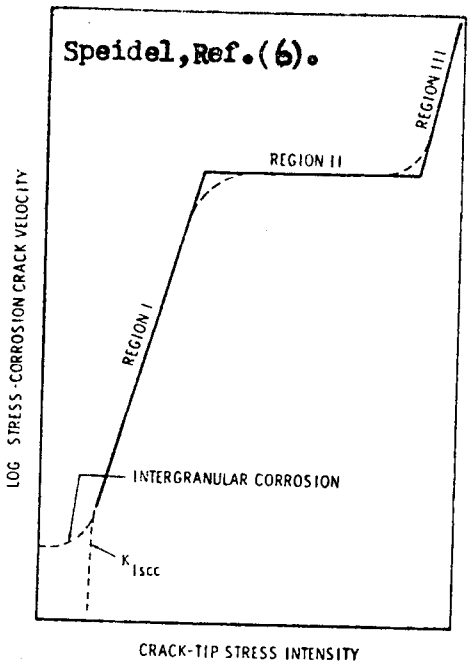

Fig. 26 Schematic representation of the influence of stress intensity on SC crack velocity

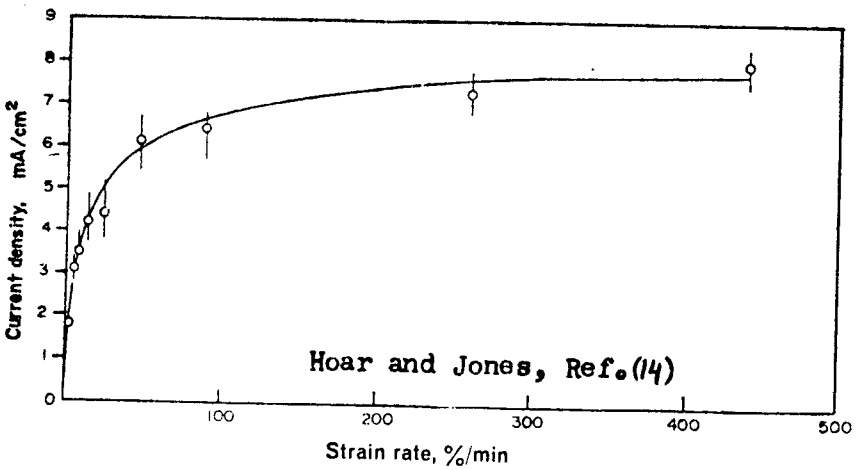

FIG. 27 Limiting density on yielding specimens.
0·1% C steel. 10M NaOH. 121°C. —0.700 V(she).

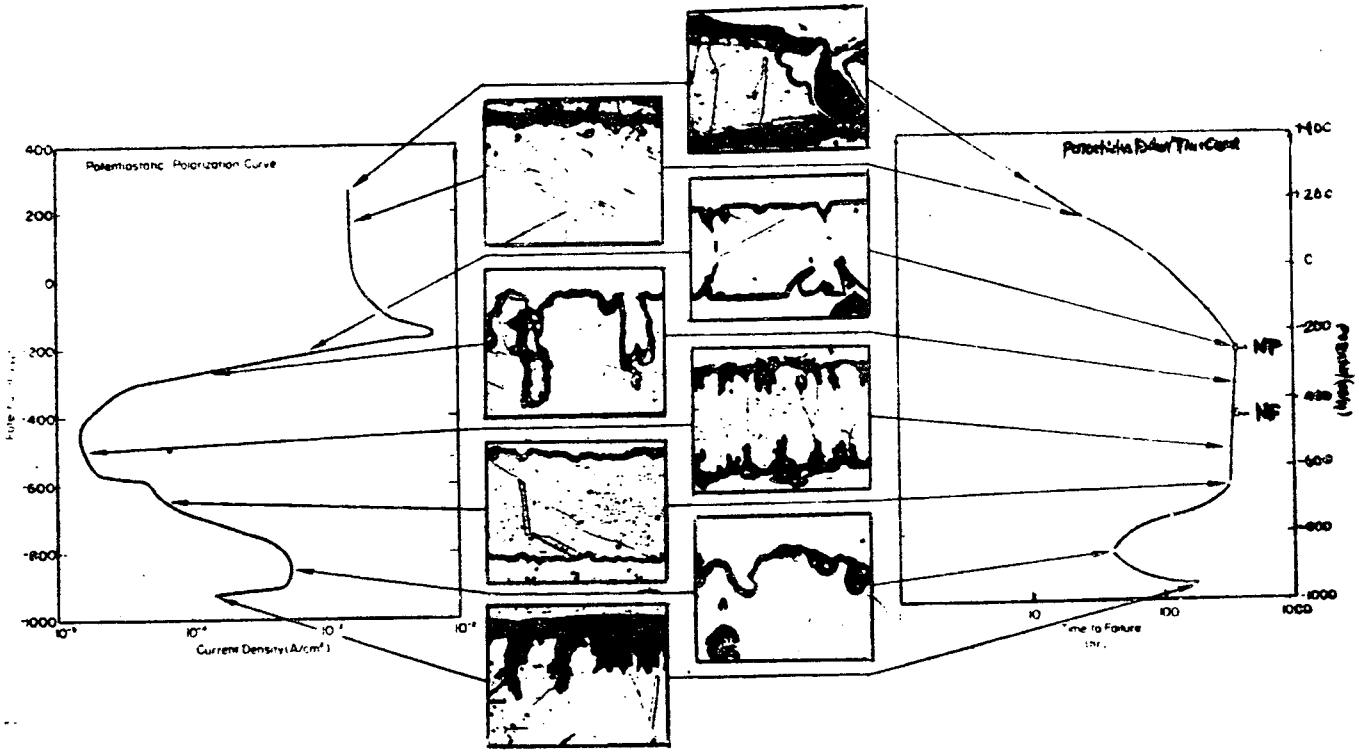

Fig. 28 Morphology of stress corrosion cracks in type 304 steel exposed to boiling 60% NaOH solution. Photomicrographs are related to polarization curve and time to failure curve for 304 steel in this environment. (After Subrahmanayam and Staehle 23)

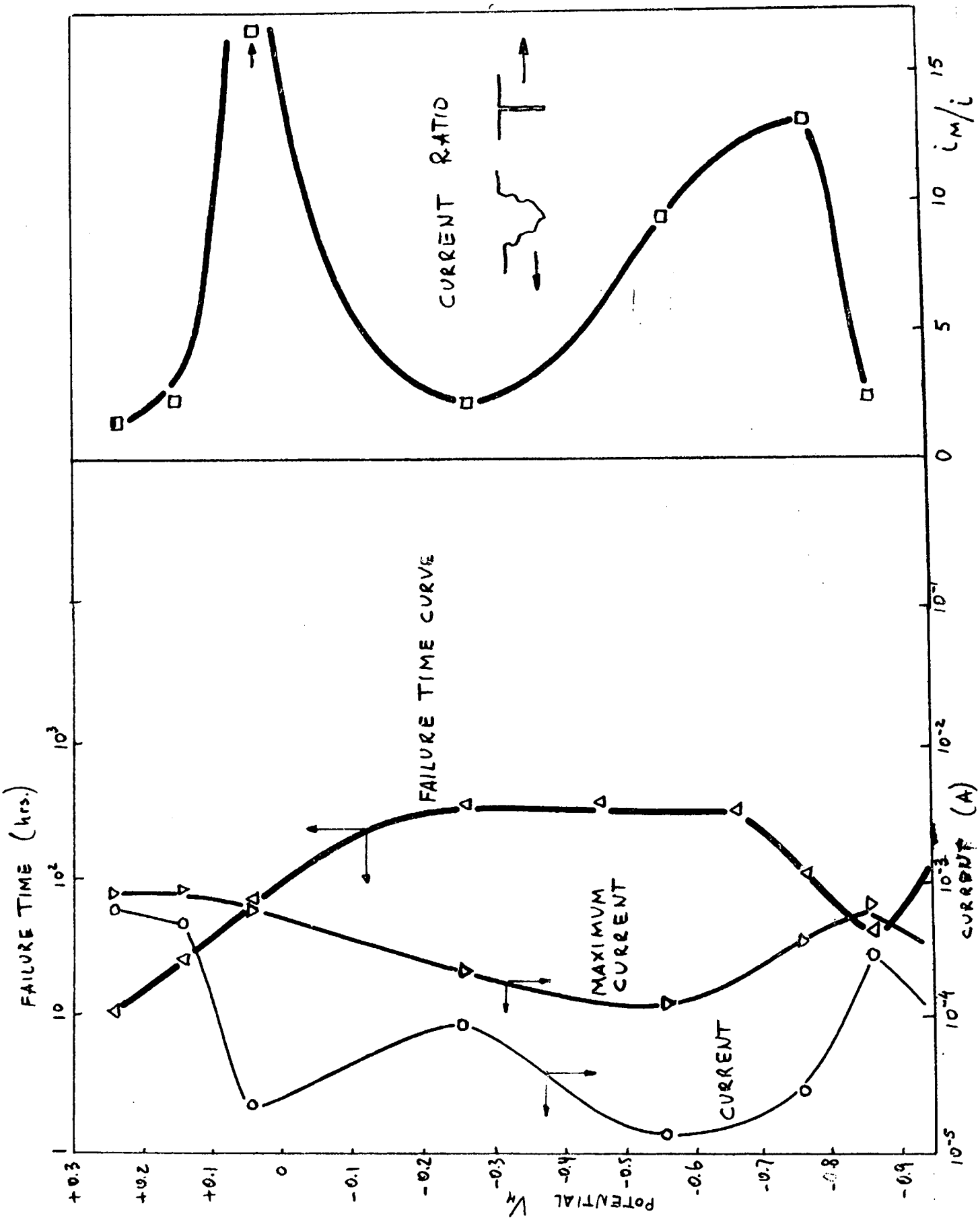

FIGURE 29.SCC of AISI 304 in boiling 60% NaOH solution.
Subrahmanayam and Staehle (23).